Research on Chemical Intermediates (2024) 50:4105–4124
https://doi.org/10.1007/s11164-024-05358-7

Modification of crystalline graphitic carbon nitride for improve efficiency in photocatalytic destruction of volatile organic compounds (VOCs) under visible light irradiation

Vitaliy Shvalagin[1,2] · Aleksandr Kutsenko[1] · Tetyana Stara[1,3] · Polina Hlukhova[1] · Mykola Skoryk[4] · Stepan Kuchmiy[1]

Received: 22 May 2024 / Accepted: 20 July 2024 / Published online: 27 July 2024
© The Author(s) 2024

Abstract

In this study, we show that the use of a mixture of melamine and oxalic acid during the synthesis of acid-treated crystalline graphitic carbon nitride samples significantly enhances its photocatalytic activity in VOCs destruction processes. The rate of photocatalytic ethanol destruction with the participation of modified crystalline graphitic carbon nitride obtained under optimal conditions is 67.1 μmol h^{-1}, which is almost twice higher than sample synthesized in the absence of oxalic acid, and is two orders of magnitude higher than the activity of bulk g–C_3N_4. The synthesized materials were characterized using XRD, FT-IR, UV–Vis, PL, SEM, and EDXA methods. The high activity of the modified carbon nitride samples is attributed to increased light absorption in the visible region of the spectrum and better crystallinity, which can lead to more efficient separation and transport of photogenerated charges. To our knowledge, the effect of the simultaneous use of melamine and oxalic acid for obtaining acid-treated crystalline graphitic carbon nitride is, shown for the first time.

Keywords Crystalline graphitic carbon nitride · Molten salt treatment · Doped carbon nitride · Visible light · Photocatalyst · Volatile organic compounds

Abbreviations

AT-Ox-CGCN	Acid-treated oxygen-doped crystalline graphitic carbon nitride
CGCN	Crystalline graphitic carbon nitride
VOCs	Volatile organic compounds
OXA	Oxalic acid

Extended author information available on the last page of the article

Introduction

Volatile organic compounds (VOCs) are among the main air pollutants that can cause adverse health effects for people indoors. Sources of VOCsinclude furniture, finishing materials, office equipment, gaseous products of human metabolism, as well as vaporous substances emitted into the air by transport, industrial enterprises, etc., which can penetrate to indoor air and cause pollution. The various technologies available today for removing VOCs from indoor air, as reviewed in [1], have several shortcomings. In particular, the most common technology, which is based on the use of various filter materials, including activated carbon, is not effective enough when it is necessary to neutralize pollutants in very small concentrations below a few ppm.

Recently, technologies based on photocatalytic oxidation transformations of VOCs have gained the attention of researchers and practitioners, as these technologies often achieve complete mineralization to CO_2 and H_2O. Typically, the active components in such technologies are semiconductor materials. Their excitation under light leads to the generation of holes in the valence band and electrons in the conduction band and the formation with their participation of highly active oxidizing particles—radicals $^{\cdot}OH$, $^{\cdot}O^{2-}$, singlet oxygen, hydrogen peroxide, etc., which initiate the oxidation of VOC molecules [2, 3].

In addition to the photoactive inorganic semiconductor—titanium dioxide, which is most commonly used as an active component in the design of photocatalytic air purifiers, the polymer semiconductor graphitic carbon nitride (g–C_3N_4) has recently attracted attention as a photocatalyst, due its numerous advantages. This material has a relatively small band gap ($E_g = 2.7$ eV), allowing it to absorb visible light [4–6]. It is non-toxic and has high thermal and chemical resistance. Unlike metal-containing photocatalysts, the preparation of which often requires expensive metal compounds, g–C_3N_4 can be easily obtained by thermal polycondensation of cheaper precursor compounds. Due to the advantageous positioning of its allowed zones, it can serve as a photocatalyst for many practically important redox processes, in particular, the destruction of environmental pollutants [7], including VOCs [8]. In addition, when it is modified (doping with metals and non-metals, grafting various functional groups, etc.), it can be used as an active component of catalysts, sensors, and other functional materials [9–12]. However, carbon nitride is not without a number of disadvantages: small surface area, low concentration of active centers, insufficient absorption of visible light, fast recombination of charges, low mobility of charges, etc.

In our previous studies, we showed that additional thermal treatment of g–C_3N_4 in melts of KCl and LiCl salts, followed by salt washing and further activation of the resulting crystalline graphitic carbon nitride (CGCN) in an acid solution yields a material that, in addition to sensitivity to visible light and high photochemical stability, has high photocatalytic activity in the oxidation of organic compounds (ethanol and acetaldehyde) with air oxygen [13].

One approach to further increase the photoactivity of materials based on graphitic carbon nitride is doping with various heteroatoms, particularly oxygen

[14–18]. It was shown in [14] that introducing oxygen into the structure of crystalline carbon nitride significantly increases the photosensitivity of the material in the long-wave range of the spectrum. While, these materials are slightly less active in hydrogen formation under light with $\lambda \approx 400$ nm compared to undoped crystalline carbon nitride, they retain high activity under light with a wavelength of more than 500 nm in contrast to the undoped carbon nitride, which is practically inactive under such conditions [14].

In this work, we present the results of studying the effect of acid treatment of crystalline graphitic carbon nitride obtained using melamine and oxalic acid (OXA) during synthesis. This approach increases its photocatalytic activity under visible light in the gas-phase oxidation of ethanol and acetaldehyde, which are potential air pollutants.

Material and methods

Materials

We used melamine (99%), oxalic acid (≥ 99.0%), HCl (puriss. p.a., ≥ 37%) from Sigma-Aldrich, KCl (≥ 99.5%) from Merck, LiCl (99%) from Thermo scientific, and ethanol (96% (v/v), extra pure) from Khimlaborreaktiv. The reagents were used without additional purification.

Synthesis

Bulk graphitic carbon nitride—g–C_3N_4 and Ox–g–C_3N_4 samples (where x is the mass percentage of OXA during synthesis) were obtained by calcining, respectively, melamine and a mixture of melamine and OXA at 550 °C for 2 h in the presence of air oxygen. Next, the obtained materials were cooled to room temperature and ground to a powdery state in a ball mill. As a result, powders were obtained, the color of which gradually changed from yellow to dark brown with an increase in the content of OXA from 0 to 30 wt. % in mixture of melamine and OXA during synthesis.

Crystalline graphitic carbon nitride—CGCN and Ox-CGCN samples (where x is the mass percentage of OXA during synthesis of Ox–g–C_3N_4) were obtained from previously synthesized bulk carbon nitrides. In a typical procedure, g–C_3N_4 or Ox–g–C_3N_4 (1.2 g), KCl (3.3 g) and LiCl (2.7 g) were ball milled. The obtained homogeneous mixture was placed in a glass flask, heated in a muffle furnace to 550 °C and kept at this temperature for 4 h. After cooling to room temperature, distilled water was added to the mixture and stirred thoroughly until the salts were completely dissolved. The obtained suspension was centrifuged at 5000 rpm to separate the sediment from the salt solution. This procedure was repeated several times to completely remove dissolved salts. Finally, the product was washed with ethanol, separated by centrifugation, and dried in air at 60 °C.

Acid-treated crystalline graphitic carbon nitride—AT-CGCN and AT-Ox-CGCN samples (where x is the mass percentage of OXA during synthesis of Ox–g–C_3N_4) were obtained by stirring of CGCN and Ox-CGCN samples in 0.1 M aqueous HCl solution for 2 h, followed by washing of the samples with distilled water and ethanol, after which they were dried at 60 °C in air.

Characterization

The diffractograms of the samples were recorded in the range of angles from 2θ = 5–50° using a Bruker D8 Advance X-ray diffractometer with Kα radiation of the copper line ($\lambda = 0.1540$ nm) with a scanning speed of 5 degrees/min. Infrared (IR) spectra were recorded in the frequency range of 3800–500 cm^{-1} using a Perkin Elmer spectrum one spectrometer. The samples were finely ground with KBr (1:100 ratio) and pressed at 10 MPa. Diffuse reflectance spectra were recorded using an integral sphere on a Specord 210 spectrophotometer in the wavelength range of 400–700 nm. The resulting spectra were transformed into absorption spectra using the Kubelka–Munk function. The photoluminescence and excitation luminescence spectra of the materials were recorded on a Perkin-Elmer LS55 luminescence spectrometer. Scanning electron microscopy (SEM) studies were performed using a Mira3 Tescan microscope equipped with an attachment for X-ray energy dispersive analysis Oxford X-max 80 mm^2, at an accelerating voltage of 5–20 kV.

Photocatalytic experiments

Research on the photocatalytic destruction of ethanol was carried out in a sealed 140 cm^3 glass reactor with a membrane for ethanol injection and sampling. A photocatalyst sample (30 mg) was pressed on copper substrate (1*3 cm) and fixed inside the glass reactor. Liquid ethanol (2 µl) was then injected into the reactor using a microsyringe. The reaction mixture was stirred for about 2 h to evaporation of ethanol and establish the adsorption–desorption equilibrium. The sample was then irradiated with lens-focused light from a high-pressure mercury lamp (DRSH-1000), from the spectrum of which light with $\lambda > 410$ nm was extracted using a cut-off glass light filter ZhS-10. Concentrations of initial ethanol and organic products (acetaldehyde) in the gas-phase were determined during irradiation using a Thermo Fisher Scientific TRACE 1310 gas chromatograph with an FID detector and an Agilent DB-WAX column. A scheme of the reaction set up is shown in Fig. S1.

Results and discussion

Study of the structural and optical characteristics of the obtained materials

In the diffractogram of bulk g–C_3N_4 obtained by pyrolysis of melamine (Fig. 1a), there is a reflection at 2θ = 27.3°, which corresponds to the interplanar distance between monolayers $d_{002} = 0.326$ nm. This value is in the range typical for g–C_3N_4

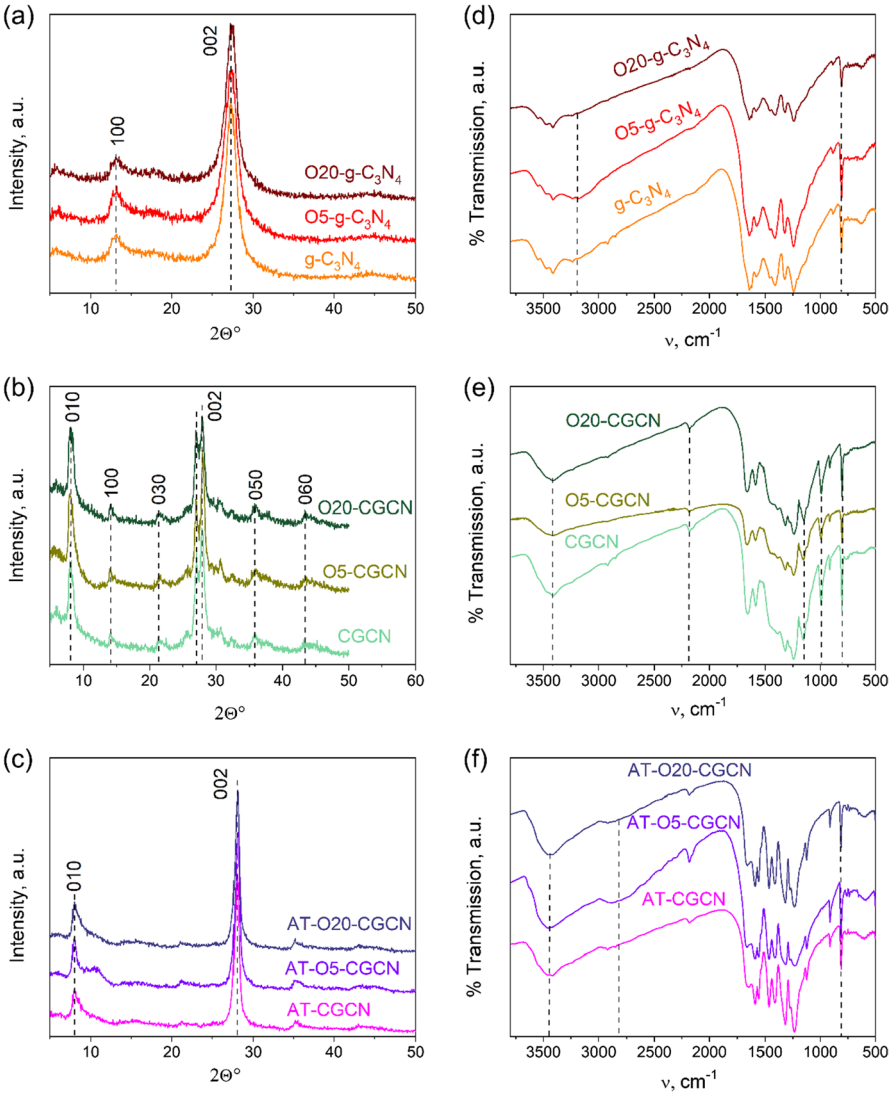

Fig. 1 Diffraction patterns and IR spectra of g–C_3N_4, O5–g–C_3N_4, O20–g–C_3N_4 (**a**, **d**); CGCN, O5-CGCN, O20-CGCN (**b**, **e**) and AT-CGCN, AT-O5-CGCN, AT-O20-CGCN (**c**, **f**) samples, respectively

from 0.319 to 0.326 nm [19–22]. The reflex at 2θ = 13.1° (index 100) corresponds to the periodicity (0.675 nm) between heptazine fragments alternating within one monolayer [20, 21].

As shown in Fig. 1a, pyrolysis of melamine in the presence of 5% and 20% of OXA does not lead to significant changes in the diffractograms of the obtained samples. This suggests that OXA has only a slight influence on the crystalline structure of the materials.

In the diffractograms of CGCN, O5-CGCN and O20-CGCN samples, obtained by additional molten salt treatment of g–C_3N_4, O5–g–C_3N_4, and O20–g–C_3N_4, respectively, an intense reflex is observed at 2θ = 28.0° (d = 0.318 nm) (Fig. 1b). This indicates a decrease in the interlayer distance from d_{002} = 0.326 nm for g–C_3N_4 to d_{002} = 0.318 nm for CGCN. This may indicate an increase in the planarity of carbon nitride layers, leading to enhanced electronic interaction between the π-systems of neighboring layers and their convergence [22]. It should be noted that in the diffractograms of CGCN, O5-CGCN, and O20-CGCN there are several much weaker reflections at different values of 2θ. According to [23], reflections at 2θ ≈ 14°, 21°, 36°, 43° correspond to X-ray diffraction on the (100), (030), (050), and (060) planes of carbon nitride crystals, respectively. This indicates improved crystallinity in the CGCN, O5-CGCN, and O20-CGCN samples obtained by thermal treatment of the initial bulk g–C_3N_4, O5–g–C_3N_4, and O20–g–C_3N_4 in the melt of the LiCl + KCl eutectic mixture. In the diffractograms of CGCN samples, there is also a reflection at 2θ = 27.0°, which indicates the presence of several polytypes with different interlayer packing in the obtained materials [24]. Additionally, an intense reflex at 2θ = 8.1° (d = 1.09 nm) is recorded in the X-ray patterns of CGCN samples. The reason for its appearance may be a better arrangement of tri-s-triazine blocks within the monolayer [25–27], as well as the incorporation of potassium atoms, which are larger than C and N, into the g–C_3N_4 lattice [28]. An increase in the OXA content during the synthesis of the initial Ox–g–C_3N_4 samples does not lead to significant changes in the X-ray patterns of the resulting Ox-CGCN crystalline samples.

Considering that crystalline samples of carbon nitride show activity in hydrogen evolution reaction only in the presence of acid [29], and that acid-treated CGCN samples exhibit significantly higher activity and stability in the oxidation of organic substrates [13], within the framework of this work also the effect of acid treatment of OXA modified crystalline carbon nitride samples on their spectral and photocatalytic properties was investigated.

In the diffractograms of all acid-treated samples (AT-CGCN, AT-O5-CGCN and AT-O20-CGCN) (Fig. 1c), clear reflections are observed at 2θ = 8.0° and 28.0° (d = 1.1 and 0.318 nm, respectively). However, the reflection at 2θ = 27.0° (d = 0.328 nm) present in the diffractograms of untreated samples, disappears (Fig. 1b). This may be due to the removal of potassium ions from the interlayer space of the material. The intense reflections at 2θ = 28.0°, which characterize the distance between adjacent monolayers connected by van der Waals forces, are shifted toward large angles in the diffractograms of AT-CGCN, AT-O5-CGCN, and AT-O20-CGCN samples compared to g–C_3N_4 (2θ = 27.25°). This shift indicates a decrease in the distance between layers the acid-treated crystalline samples and an increase in their planarity [22].

In addition, the narrowing and increase in the intensity of the reflex at 2θ = 28.0° in the diffractograms of AT-CGCN, AT-O5-CGCN and AT-O20-CGCN further indicate an increase in the degree of orderliness of their layered structure. It should be noted that increasing OXA content during the synthesis does not lead to a change diffractograms of acid-treated CGCN (Fig. 1c).

In the IR spectra of g–C_3N_4, O5–g–C_3N_4, and O20–g–C_3N_4 samples, there is a band at 810 cm^{-1}, which is the so-called "fingerprint" of triazine and heptazine

heterocycles and is caused by N–C=N bonds deformation vibrations in these compounds (Fig. 1d) [30, 31]. In addition, in the IR spectra of all samples, a set of bands at 1700–1200 cm^{-1} is observed, which are characteristic of tri-s-triazine derivatives [31]. A decrease in the intensity of these bands in the O20–g–C_3N_4 spectrum indicates a reduction in the area of the conjugated heterocyclic system and indicates a less ordered crystal structure of the sample. In all samples in the range of 3000–3500 cm^{-1} there is a broad band due to valence fluctuations of OH groups of adsorbed water and residual NH_2 (NH) groups of polyheptazine. At the same time, the intensity of this band for the O20–g–C_3N_4 sample is significantly lower, which may indicate a lower content of NH_2 (NH) groups with a high content of OXA during synthesis.

In the IR spectra of CGCN, O5-CGCN, and O20-CGCN samples (Fig. 1e), a broad band in the range 3000–3600 cm^{-1} with a maximum at 3420 cm^{-1} is observed. This is due to valence vibrations of OH groups of adsorbed water, as well as residual amino groups. In the spectra, there is no band with a maximum at about 3190 cm^{-1}, characteristic of bulk carbon nitride samples (Fig. 1d). According to [32], this may indicate denser packing of heptazine blocks with the removal of part of the excess amino groups, between which the formation of a hydrogen bond is possible. In addition, a band at 2168 cm^{-1} appears in the IR spectra of crystalline samples (Fig. 1, e), which corresponds to the oscillations of terminal C≡N groups, which arise as a result of the loss of ammonia during thermal treatment [25–27]. In the spectra of all CGCN samples, there are also bands at 990 and 1150 cm^{-1}, which can be attributed to symmetric and asymmetric vibrations of metal-NC_2 groups, respectively [28], which may be evidence of the inclusion of potassium atoms in the composition of crystalline samples. In the IR spectra of CGCN, O5-CGCN and O20-CGCN, there is also a clear band at 808 cm^{-1}, due to the deformation fluctuations of the N–C=N bonds in the heterocycles of the triazine and heptazine series [4, 27]. A set of bands at 1700–1200 cm^{-1} is also observed in all spectra, which can be attributed to vibrations of the tri-s-triazine lattice [4], as well as deformation vibrations of water molecules.

It should be noted that the IR spectra of the CGCN, O5-CGCN, and O20-CGCN samples are similar to each other and do not contain bands that could indicate the presence of a significant number of oxygen-containing groups in their composition.

As can be shown from Fig. 1f, in the IR spectra of AT-CGCN, AT-O5-CGCN, and AT-20-CGCN samples obtained after acid treatment of CGCN, O5-CGCN and O20-CGCN samples, the bands at 1150 and 990 cm^{-1} disappear, which correspond to symmetric and asymmetric vibrations of NC2-metal groups [28]. This may indicate the removal of potassium ions, which are incorporated into the structure of carbon nitride during the treatment of the original g–C_3N_4 in the melt of KCl and LiCl salts. Since, according to [25–27], dopant metals form an ionic bond with the CGCN matrix, it is natural to assume that potassium ions are replaced by protons. In addition, acid treatment of CGCN, O5-CGCN and O20-CGCN samples leads to an increase in the intensity of absorption bands characteristic of carbon nitride in the range of 1200–1650 cm^{-1} (Fig. 1f), which correspond to valence vibrations of aromatic CN-bonds of condensed nitrogen-containing heterocycles, which may be associated with an increase in the degree of their ordering.

The electronic absorption spectrum of g–C_3N_4 is characterized by a long-wave edge of the absorption band at about 455 nm (Fig. 2a), which is quite typical for such a material. The introduction of 5% OXA during the synthesis leads to an increase in the absorption of the sample in the entire visible range of the spectrum and a bathochromic shift of the long-wave edge of the absorption band to about 470 nm (Fig. 2a), which may indicate the incorporation of oxygen into the carbon nitride structure. A further increase in the content of oxalic acid to 20% during the synthesis of carbon nitride leads to a significant increase in absorption intensity and a shift of the long-wave absorption edge to about 570 nm (Fig. 2a).

The electronic absorption spectra of CGCN, O5-CGCN, and O20-CGCN samples, obtained by additional treatment of bulk g–C_3N_4, O5–g–C_3N_4, and O20–g–C_3N_4 in molten salts are shown in Fig. 2b. As can be seen, such treatment leads to the formation of bands with an absorption edge around 460 nm in the spectra. However, oxygen-doped samples of crystalline carbon nitride O5-CGCN and O20-CGCN (Fig. 2b), in addition to the main band, exhibit a broad absorption band in the entire visible range. This broad band is especially clearly seen in the case of the O20-CGCN sample and may indicate on the incorporation of oxygen-containing groups into the structure of the samples. However, as can be seen from the Fig. S2a,

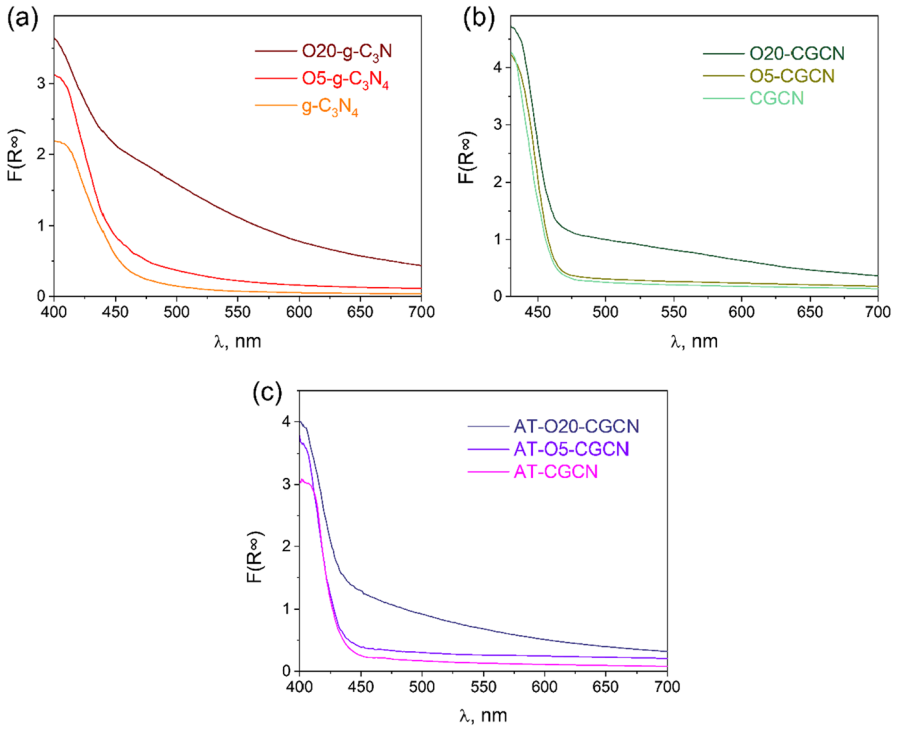

Fig. 2 Absorption spectra of the samples g–C_3N_4, O5–g–C_3N_4, O20–g–C_3N_4 (**a**), CGCN, O5-CGCN, O20-CGCN (**b**) and AT-CGCN, AT-O5-CGCN, AT-O20-CGCN (**c**)

the bandgap (*Eg*) of these materials remains nearly unchanged at 2.84 eV. The increased absorption in the visible region is likely due to the formation of defects in the semiconductor's band gap. Comparing the absorption spectra of CGCN, O5-CGCN, and O20-CGCN samples with the spectra of g–C_3N_4, O5–g–C_3N_4, and O20–g–C_3N_4, respectively, allows us to make the following conclusions: treatment in molten salts increases the absorption intensity of the samples in the range of $\lambda < 460$ nm with the formation of a clearer edge of the absorption band, consistent with literature data [33]; the salts melt treatment of the oxygen-doped samples leads to slight decrease in the absorbance in the range $\lambda > 460$ nm, which may be related to the removal of oxygen-containing groups from the surface of the samples during thermal treatment. Notably, there is a slight decrease in *Eg* to 2.76, 2.73, and 2.72 eV during the transition from CGCN to O5-CGCN and O20-CGCN, respectively (Fig. S2b).

As can be seen from the absorption spectra of acid-treated crystalline carbon nitride samples (AT-CGCN, AT-O5-CGCN, and AT-O20-CGCN) (Fig. 2c), the edge of the absorption band in all cases undergoes a hypsochromic shift relative to the crystalline samples of carbon nitride prior to acid treatment and is around 435 nm for the AT-CGCN and AT-O5-CGCN sample and around 440 nm for the AT-O20-CGCN sample. This shift of the absorption edge corresponds to a decrease in E_g from 2.94 to 2.90 eV when transitioning from AT-CGCN and AT-O5-CGCN to AT-O20-CGCN, respectively (Fig. S2c). With an increase in the content of the modifier, in addition to a slight bathochromic shift of the edge of the absorption band relative to the undoped sample, there is also absorption in the entire visible region of the spectrum, the intensity of which increases with an increase in the concentration of OXA during synthesis. Absorption in the visible range in the case of OXA modified samples practically does not change after their treatment in acid, which may indicate the acid stability of oxygen-containing groups formed in the process of sample synthesis.

The increase in the oxygen content in the AT-Ox-CGCN samples, synthesized using a mixture of melamine and OXA, was confirmed using the EDX method (Table 1). As can be shown from Table 1, an increase in OXA content during synthesis leads to a corresponding increase in the oxygen content in the carbon nitride samples, consistent with the literature [18].

Figure 3a, b show the photoluminescence (PL) spectra of bulk g–C_3N_4, CGCN, and AT-CGCN samples synthesized without OXA. As can be seen, g–C_3N_4 emits intensively in the blue-green range with $\lambda_{max} \approx 460$ nm. According to our previous results [34], the PL band of g–C_3N_4 contains at least two components. The short-wave component is attributed to the direct interband radiative recombination of

Table 1 Content of the elements (at.%) in carbon nitride samples according to EDXA data

Sample	C	N	O	Cl	K
AT-CGCN	44.66	52.68	0.55	1.51	0.60
AT-O5-CGCN	45.62	52.94	0.77	0.33	0.34
AT-O20-CGCN	39.46	59.05	1.49	–	–

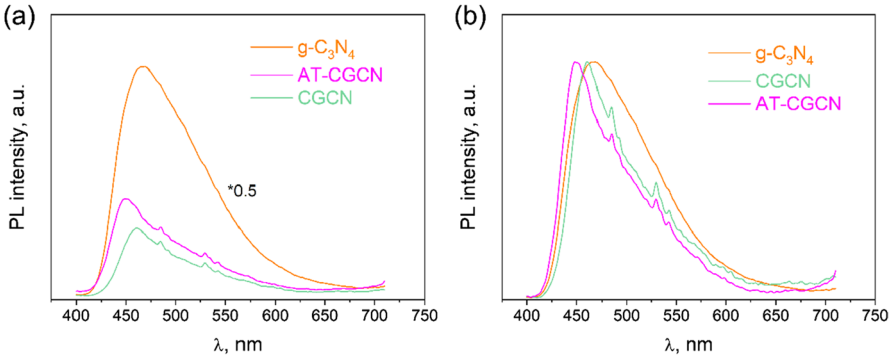

Fig. 3 **a** PL spectra of g–C_3N_4, CGCN and AT-CGCN samples. **b** Normalized spectra of the corresponding samples. $\lambda_{exc} = 370$ nm. Narrow peaks in the PL spectra at ~480 and ~530 nm are artifacts of the measuring device

photogenerated electrons and holes, while the long-wave component is due to the recombination of carriers on structural defects of the periodic structure of g–C_3N_4 monolayers. Treatment of samples in molten salts (CGCN) and acid solution (AT-CGCN) leads to a significant decrease in PL intensity for both components. This reduction is primarily due to a decrease in particle size and an increase in the surface area of the material during the treatment process [13]. Smaller sizes and a larger surface area ensure a faster release of photogenerated charge carriers to the surface of the particles, thereby reducing the rate of their recombination. In addition, as can be seen from Fig. 3b, in the PL spectra of CGCN and AT-CGCN, the contribution to the integral samples PL intensity of components associated with defects decreases. This indicates a decrease in the number of defects involved in radiative recombination and may be associated with an increase in the planarity of the layers in the samples after their treatment, which is consistent with X-ray diffraction data.

Figure 4 shows the PL and excitation luminescence (EL) spectra of g–C_3N_4, O5–g–C_3N_4, and O20–g–C_3N_4 samples. As can be seen (Fig. 4a, b), an increase of OXA content during synthesis leads to a decrease in the PL intensity of the samples due to both components. At the same time, there is an increase in the contribution to the integral PL of the components associated with radiative recombination at defects, which is clearly manifested in the spectra of the O20–g–C_3N_4 sample. Thus, the synthesis of carbon nitride in the presence of oxalic acid results in the formation of additional defects in it, connected, in particular, with the formation of oxygen-containing groups.

Three bands are present in the EL spectra of g–C_3N_4 and O5–g–C_3N_4 samples (Fig. 4c, d), which indicates the presence of at least three PL excitation centers in them. Bands with maxima at ~280, 370, and 440 nm can be attributed to $\sigma-\sigma^*-$, $\pi-\pi^*-$ transitions, and electronic transitions involving defect states, respectively [34]. With an increase in the content of oxalic acid, a decrease in the intensity of the band associated with defects is shown (Fig. 4d). At a concentration of 20% of oxalic acid (sample O20–g–C_3N_4), the EL spectra of the sample contains only two bands, which indicates a decrease in the number of EL centers.

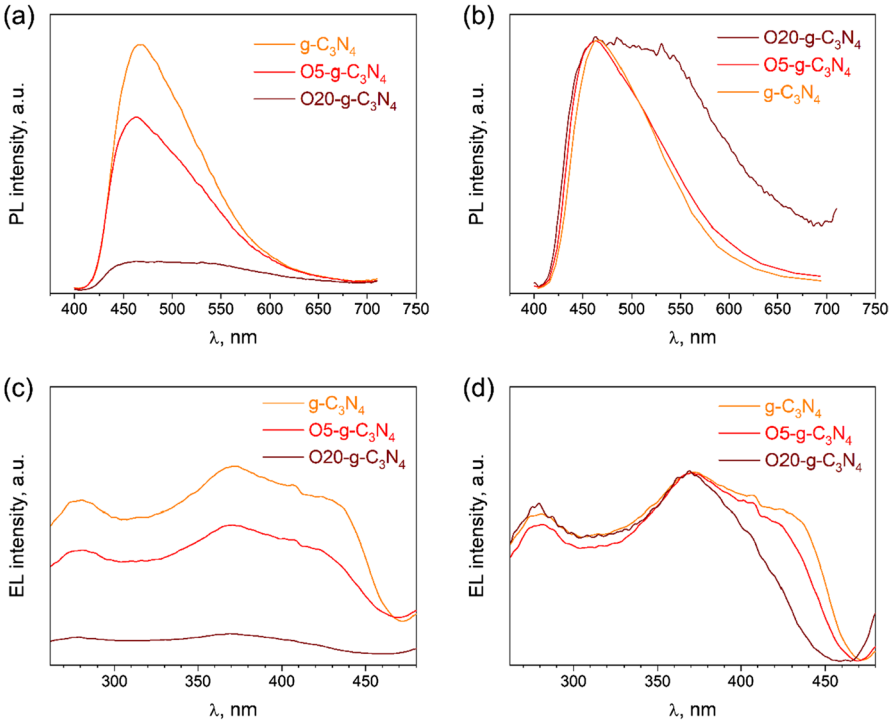

Fig. 4 Spectra of PL (**a**), normalized PL (**b**), EL (**c**) and normalized EL (**d**) of g–C_3N_4, O5–g–C_3N_4 and O20–g–C_3N_4 samples

Doping CGCN samples with OXA leads to a drop in their PL intensity (Fig. 5a). At the same time, there is an increase in the relative contribution to the integral PL of long-wavelength components associated with recombination involving defects, which become dominant in the spectrum of the O20-CGCN

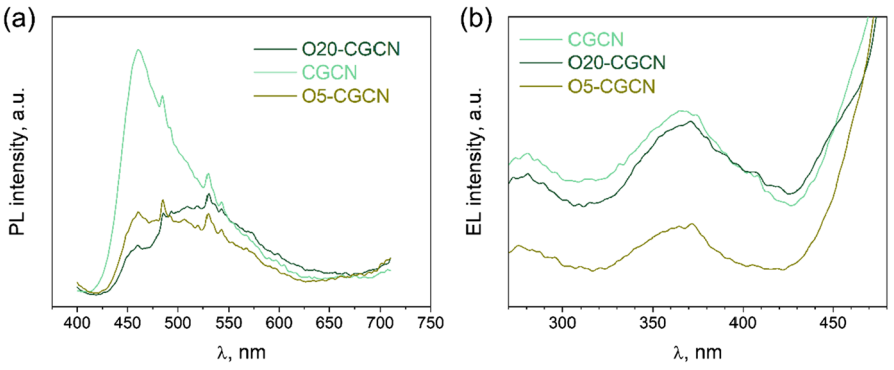

Fig. 5 PL spectra (**a**) and EL spectra (**b**) of CGCN, O5-CGCN and O20-CGCN samples. $\lambda_{exc} = 370$ nm, $\lambda_{em} = 500$ nm. Narrow peaks in the PL spectra at ~480 and ~530 nm are artifacts of the measuring device

sample. In the EL spectra of CGCN (Fig. 5b), there are two bands with positions at ~280 and 370 nm. The absence of the third ~440 nm band is associated with the presence of potassium ions in these samples [34]. At the same time, OXA doping does not significantly affect the EL spectra of CGCN samples.

Figure 6 shows the PL and EL spectra of samples AT-CGCN, O5-AT-CGCN, O20-AT-CGCN obtained by acid treatment of CGCN, O5-CGCN, O20-CGCN. As can be seen, when using 5% and 20% of OXA during the synthesis of samples, their PL intensity after acid treatment first decreases and then increases. At the same time, the emission of samples O5-AT-CGCN, O20-AT-CGCN is predominantly attributed to recombination at defects. A significant increase in the number of defects involved in radiative recombination in the O20-AT-CGCN sample is noteworthy (Fig. 6a).

The EL spectra of AT-CGCN samples contains an intense band at ~440 nm (Fig. 6b), the appearance of which can be caused by the removal of potassium during acid treatment, the release of defects associated with it, as well as the protonation of groups that participate in PL excitation, as evidenced by the higher content of hydrogen atoms in AT-CGCN samples compared to CGCN [13, 34]. On the other hand, this band is practically absent in the EL spectra of samples O5-AT-CGCN, O20-AT-CGCN. This indicates that as a result of OXA modification, such PL excitation centers are blocked. However, their disappearance is accompanied by the appearance of other PL excitation centers, which correspond to the shoulder at ~390–400 nm (Fig. 6 b).

Thus, OXA modification of all investigated samples of carbon nitride leads to a decrease in PL intensity, an increase in the number of defects involved in radiative recombination, and a change in the number and composition of PL excitation centers. The decrease in PL intensity may indicate improved separation efficiency of photogenerated carriers, which is observed when g–C_3N_4 is doped with oxygen [15–17]. On the other hand, the incorporation of oxygen into carbon nitride can lead to a changing of its structure, the appearance of non-radiative recombination centers and a decrease in PL intensity.

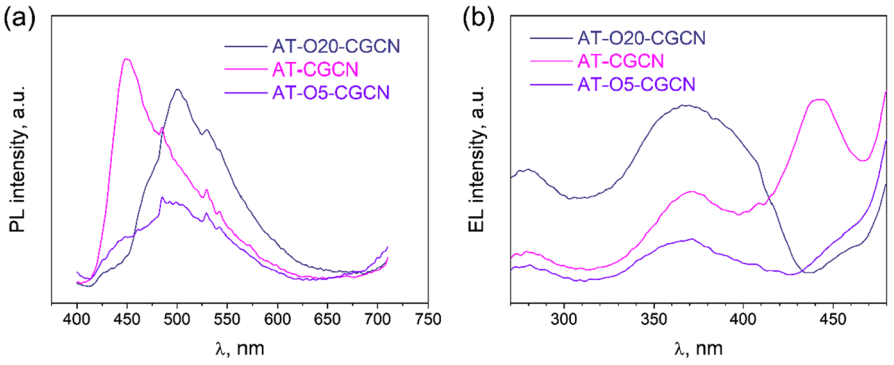

Fig. 6 PL spectra (**a**) and EL spectra (**b**) of AT-CGCN, O5-AT-CGCN and O20-AT-CGCN samples. λ_{exc} = 370 nm, λ_{em} = 500 nm. Narrow peaks in the PL spectra at ~480 and ~530 nm are artifacts of the measuring device

As can be seen from the SEM microphotographs (Fig. 7a, b), the g–C_3N_4 sample consists of spongy micrometer particles with a wall thickness of about 50 nm.

Additional thermal treatment of g–C_3N_4 in salt melts leads to a significant change in its morphology, namely to the formation of particles with a length of several hundred nanometers and a thickness of about 50 nm (Fig. 8a, b), which is consistent with [25].

This indicates that additional treatment of the bulk g–C_3N_4 in melts of lithium and potassium salts leads not only to an increase in the crystallinity of the original material, but also to its delamination and reduction of lateral dimensions to the nanometer range. It should be noted that the use of OXA in the synthesis does not significantly affect the morphology of both bulk (g–C_3N_4 and O5–g–C_3N_4 samples) (Fig. 7a–d) and crystalline samples (CGCN and O5-CGCN) (Fig. 8a–d). As can be seen from the microphotographs (Fig. 9), acid treatment of CGCN and O5-CGCN also does not lead to a significant change in their morphology. Like the original

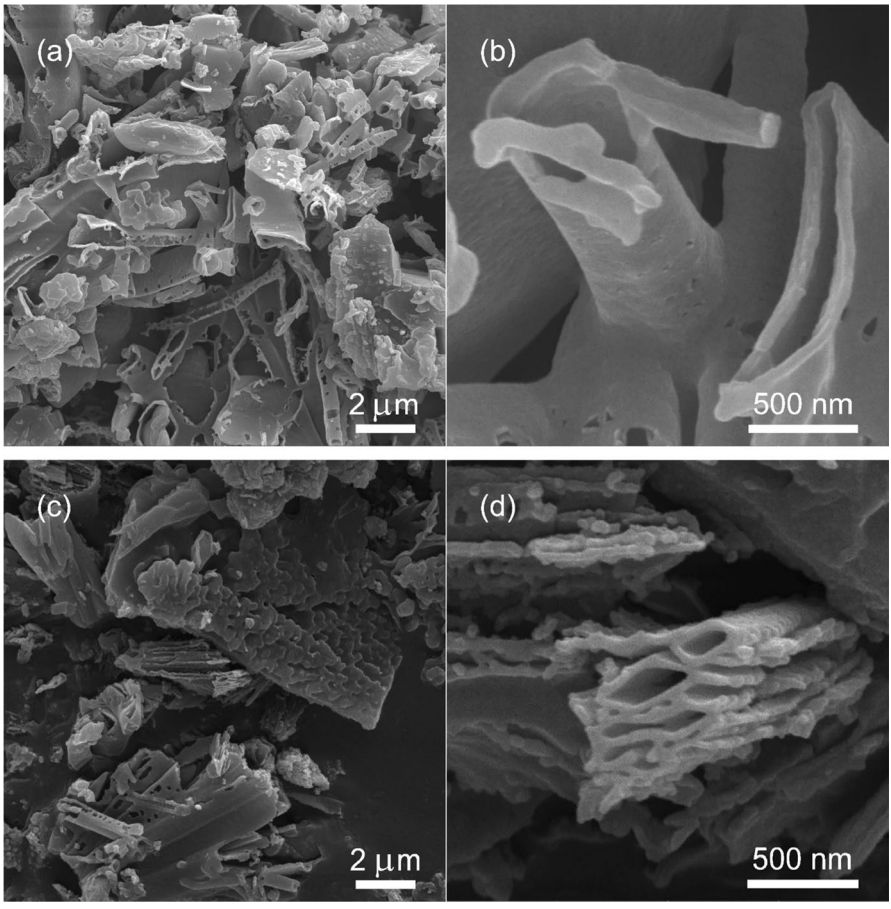

Fig. 7 SEM micrographs of g–C_3N_4 (**a**, **b**) and O5–g–C_3N_4 (**c**, **d**) samples at different magnifications

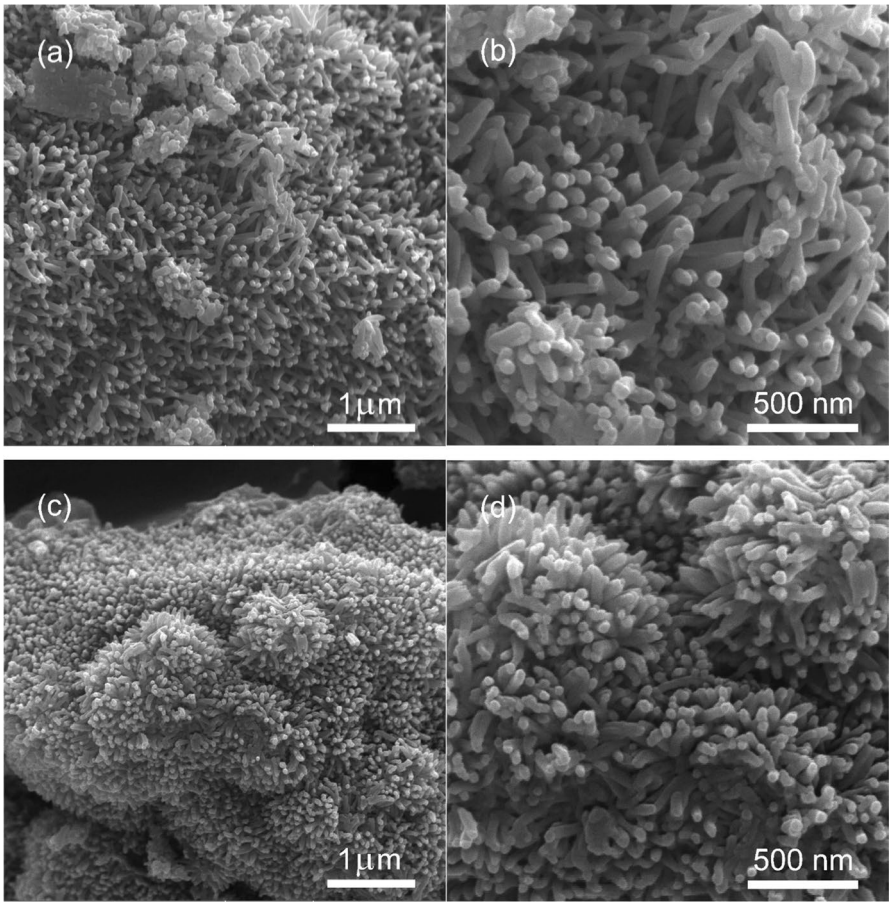

Fig. 8 SEM micrographs of CGCN (**a, b**) and O5-CGCN (**c, d**) samples at different magnifications

CGCN and O5-CGCN, the AT-CGCN and AT-O5-CGCN samples consist mainly of particles with a length of about 300–500 nm and a width of about 50 nm. The obtained results indicate the chemical stability of crystalline graphitic carbon nitride samples, which is able to preserve its structure after treatment in acid solution.

Photocatalytic properties of synthesized samples

The photocatalytic activity of the obtained materials was studied in the reaction of gas-phase oxidation of ethanol with oxygen in air under visible light irradiation ($\lambda_{irr} > 400$ nm). Kinetic curves of changes in concentrations of ethanol and the intermediate product acetaldehyde during irradiation of a closed system containing a photocatalyst and C_2H_5OH in the presence of air oxygen are shown in Fig. 10a. It should be noted that neither the bulk carbon nitride obtained from melamine, nor the samples obtained by calcining a mixture of melamine and oxalic acid, show

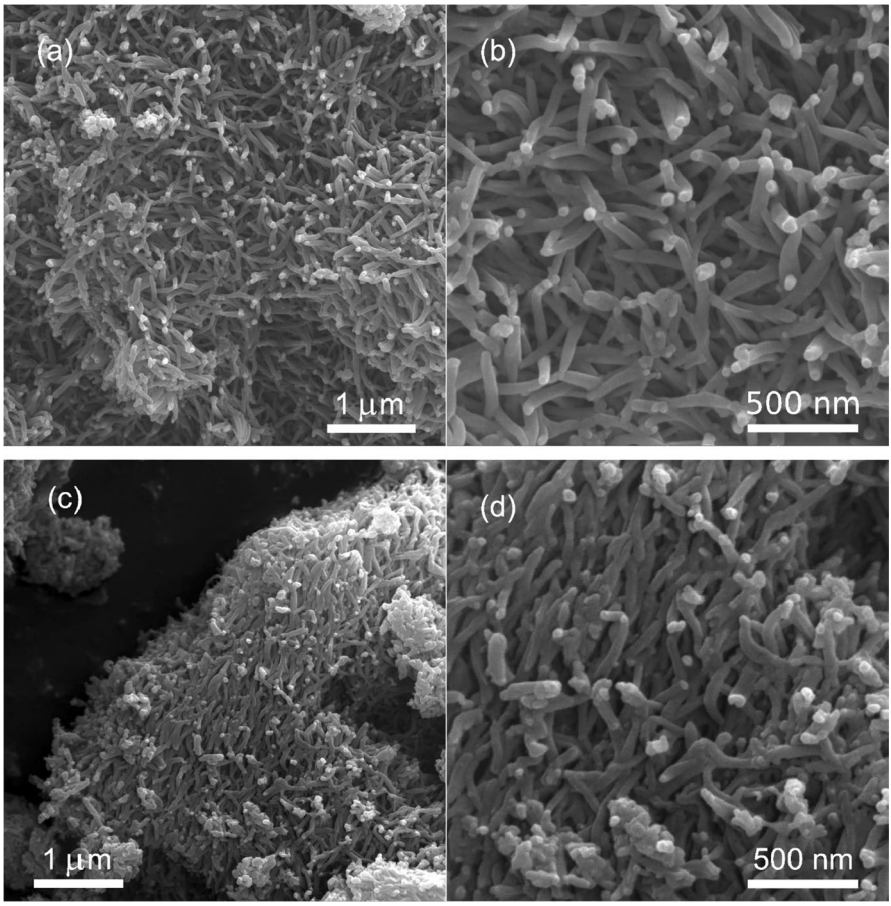

Fig. 9 SEM micrographs of AT-CGCN (**a**, **b**) and AT-O5-CGCN (**c**, **d**) samples at different magnifications

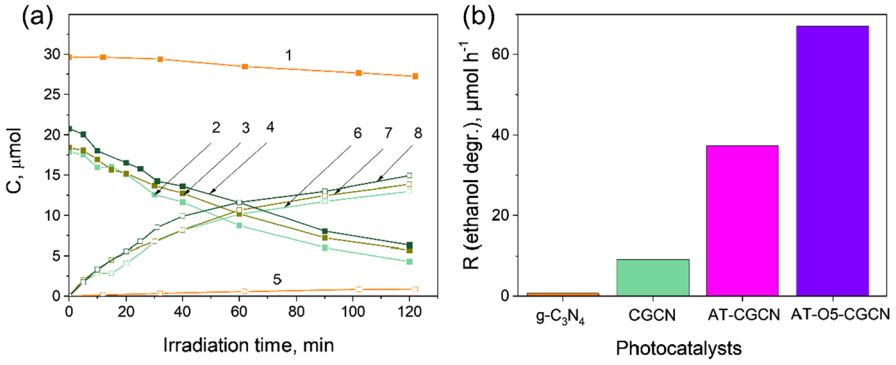

Fig. 10 **a** Kinetic curves of photocatalytic ethanol oxidation (curves 1–4) and acetaldehyde formation (5–8) with the participation of g-C_3N_4 (curves 1, 5), CGCN (2, 6), O5-CGCN (3, 7) and O20-CGCN (4, 8). **b** Rate of alcohol degradation in the presence of some obtained photocatalysts. $\lambda_{irr.} > 400$ nm

high photocatalytic activity in the investigated process. This may be due to their low crystallinity, the presence of a significant number of defects—recombination centers of photogenerated charges, and the absence of active centers on the surface. In addition, irradiation of ethanol vapor in our system without a photocatalyst or maintaining the photocatalyst in the presence of ethanol vapor without irradiation does not lead to a change in the ethanol content of the system after the absorption—desorption equilibrium is established, which is in good agreement with our previous results [13, 38]. These results confirm that ethanol oxidation during irradiation is a photocatalytic process. Instead, as can be seen from Fig. 10a, the activity of crystalline carbon nitride samples (CGCN, O5-CGCN and O20-CGCN) in the process of ethanol oxidation and acetaldehyde formation is significantly higher than that of the bulk g–C_3N_4. In particular, the rate of ethanol destruction increases by more than an order of magnitude—from 0.7 μmol h^{-1} for g–C_3N_4 to 9.2 μmol h^{-1} for CGCN (Fig. 10b).

At the same time, as can be seen from Fig. 10a (curves 2–4 and 6–8), doping of crystalline carbon nitride with oxygen practically does not affect its photocatalytic activity. The rate of ethanol destruction even slightly decreases when going from CGCN to O5-CGCN—9.2 and 8.5 μmol h^{-1}, respectively, and almost does not change when the content of oxalic acid increases to 20% in the synthesis of samples—8.7 μmol h^{-1} (Fig. 10a).

Figure 11a, b show the kinetic curves of changes in the content of ethanol (a) and acetaldehyde (b) in the reaction mixture for samples of crystalline carbon nitride treated in HCl solution (AT-CGCN and AT-Ox-CGCN samples). As can be seen, this treatment leads to a significant increase in their photocatalytic activity compared to CGCN and Ox-CGCN (Fig. 11a). In particular, the rate of photocatalytic degradation of ethanol reaches a value of 37.4 μmol h^{-1} with the participation of AT-CGCN and 67.1 μmol h^{-1} in the presence of AT-O5-CGCN, which is almost 7.5 times higher than the activity of undoped CGCN (Fig. 10b). As can be shown from Fig. 11b, the intermediate product of the conversion of ethanol—acetaldehyde, undergoes rapid photooxidation with the participation of acid-treated crystalline samples of carbon nitride, which indicates the possibility of using such photocatalytic systems for the complete oxidation of both ethanol and the more toxic acetaldehyde.

A significant increase in the photocatalytic activity of AT-O5-CGCN in the investigated process compared to undoped AT-CGCN can be explained by the inclusion of oxygen-containing functional groups in its structure, which, according to [35], have a positive effect on the photocatalytic activity of carbon nitride.

To evaluate the photocatalytic activity of materials in the process of ethanol oxidation, a number of approaches have been proposed, in particular, comparison of the alcohol consumption rate [36], photooxidation reaction rate constants [37], etc. In this study, the values of the time of complete oxidation of ethanol and the time of complete oxidation of the intermediate product (aldehyde) were used to evaluate the efficiency of photocatalysts similarly [38]. This evaluation criterion allows optimizing the search for an effective photocatalyst for complete air purification from VOCs. Using the specified approach, we investigated the effect of the content of OXA during the synthesis of samples on their photocatalytic activity in the reaction

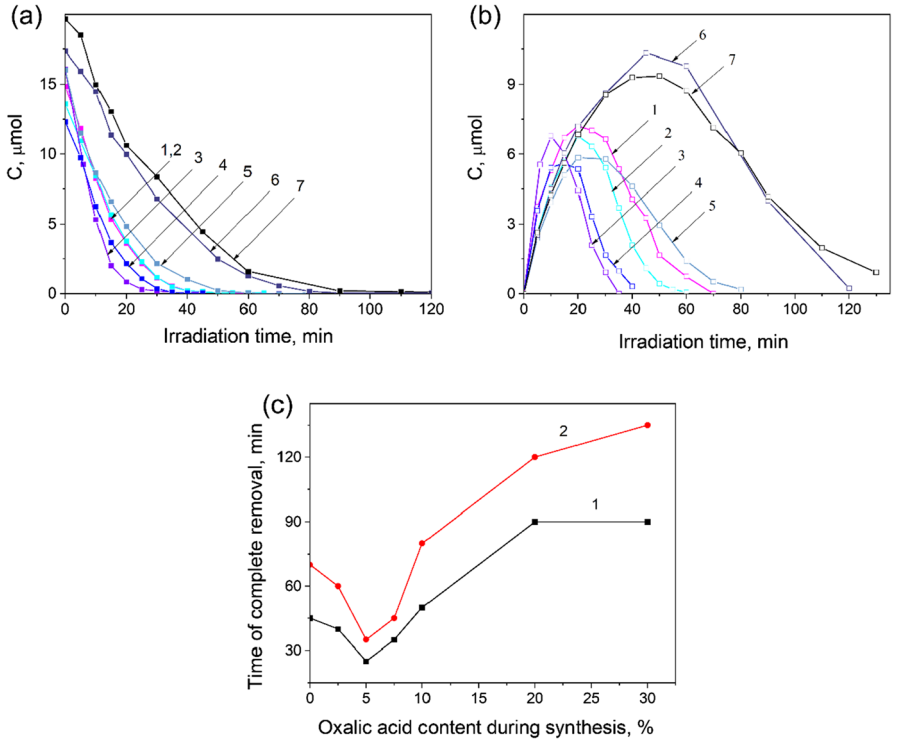

Fig. 11 Kinetic curves of ethanol oxidation (**a**) and formation and consumption of acetaldehyde (**b**) with the participation of AT-CGCN (curves 1), AT-O2.5-CGCN (2), AT-O5-CGCN (3), AT-O7.5-CGCN (4), AT-O10-CGCN (5), AT-O20-CGCN (6) and AT-O30-CGCN (7). **c** Dependence of the time of complete removal of ethanol (curve 1) and acetaldehyde (2) from the reaction mixture during irradiation on the content of OXA during photocatalyst synthesis. $\lambda_{irr} > 400$ nm

of ethanol oxidation of crystalline carbon nitride samples treated in an acid solution, the results of which are shown in Fig. 11c.

Irradiation of carbon nitride samples in an atmosphere of ethanol vapor in the presence of air leads to a gradual decrease in the content of C_2H_5OH, which is accompanied by the formation and accumulation of acetaldehyde (Fig. 11a, b). The content of acetaldehyde initially increases, and after reaching the maximum, it gradually decreases until it completely disappears in the system (Fig. 11b). As can be seen from Fig. 11c, the activity of the obtained samples of crystalline carbon nitride with an increase in the content of OXA during synthesis first increases, reaching a maximum at 5% (the minimum time for the complete destruction of ethanol and acetaldehyde is 25 and 35 min, respectively), and then decreases. When the content of OXA during synthesis is more than 10%, the activity of the samples is lower than that of undoped acid-treated crystalline carbon nitride (the time of complete destruction of ethanol and acetaldehyde is 45 and 70 min, respectively). Such a decrease in the photocatalytic activity of carbon nitride can be associated with the formation of an excess of oxygen-containing groups in its structure, which, with their high

content, can act as recombination centers of photogenerated charges and inhibit photoactivity. The obtained results indicate the need for a certain optimal content of the dopant in the structure of carbon nitride, at which its photoactivity is maximal.

Conclusions

In this work, samples of bulk graphitic carbon nitride were synthesized by pyrolysis of mixtures of melamine and OXA. It was established that the crystalline carbon nitride materials obtained from them after additional treatment in a hydrochloric acid solution show significantly higher activity in aerobic destruction of ethanol and acetaldehyde under visible light irradiation than samples synthesized without OXA after the same treatment. This increased activity may be due to enhanced light absorption following the modification of carbon nitride by OXA. The addition of OXA during the synthesis can also introduce defects in the carbon nitride structure that can act as catalytic centers and also lead to better separation of photogenerated charges, which leading to better separation of photogenerated charges and a decrease in the efficiency of unwanted electron–hole recombination. For the most active of the obtained photocatalysts (AT-O5-CGCN) the rate of ethanol destruction is 67.1 μmol h^{-1}, which is almost 2 times higher than when using unmodified AT-CGCN, and is two orders of magnitude higher than the activity of the original bulk g–C_3N_4.

Supplementary Information The online version contains supplementary material available at https://doi.org/10.1007/s11164-024-05358-7.

Acknowledgements This research was supported by the General Research Project of the L.V. Pisarzhevskii Institute of Physical Chemistry NAS of Ukraine (funded by the National Academy of Sciences of Ukraine).

Author contributions VS involved in conceptualization, investigation, writing original draft; AK involved in investigation; TS involved in investigation, writing original draft; PH involved in investigation; MS involved in investigation, SK involved in supervision. All authors read and approved the final manuscript.

Funding Open Access funding enabled and organized by Projekt DEAL.

Declarations

Conflict of interest The authors declare no competing interests.

Open Access This article is licensed under a Creative Commons Attribution 4.0 International License, which permits use, sharing, adaptation, distribution and reproduction in any medium or format, as long as you give appropriate credit to the original author(s) and the source, provide a link to the Creative Commons licence, and indicate if changes were made. The images or other third party material in this article are included in the article's Creative Commons licence, unless indicated otherwise in a credit line to the material. If material is not included in the article's Creative Commons licence and your intended use is not permitted by statutory regulation or exceeds the permitted use, you will need to obtain permission directly from the copyright holder. To view a copy of this licence, visit http://creativecommons.org/licenses/by/4.0/.

References

1. J. González-Martín, N.J.R. Kraakman, C. Pérez, R. Lebrero, R. Muňoz, Chemospere **262**, 128376 (2021)
2. A.I. Kryukov, A.L. Stroyuk, S.Y. Kuchmiy, V.D. Pokhodenko, *Nanophotocatalysis* (Kiev, Akademperiodika, 2013), p.618. (**in Russ.**)
3. J.C. Colmenares, Y.-J. Xu, *Heterogeneous Photocatalysis. From Fundamentals to Green Applications* (Springer, Berlin, 2016), p.416
4. J. Wen, J. Xie, X. Chen, X. Li, Appl. Surf. Sci. **391**, 72 (2017)
5. Y. Kang, Y. Yang, L.-C. Yin, X. Kang, G. Liu, H.-M. Cheng, Adv. Mater. **27**, 4572 (2015)
6. O.L. Stroyuk, A.E. Raevskaya, S.Y. Kuchmy, Theor. Exp. Chem. **54**, 1 (2018)
7. G. Mamba, A. Mishra, Appl. Catal. B **198**, 347 (2016)
8. S.Y. Kuchmiy, Theor. Exp. Chem. **57**, 237 (2021)
9. L. Muniandy, F. Adam, A.R. Mohamed, A. Iqbal, N.R.A. Rahman, Appl. Surf. Sci. **398**, 43 (2017)
10. P. Suja, J. Jubi, T.P.D. Rajan, G.M. Anilkumar, T. Yamaguchi, S.C. Pillai, U.S. Hareesh, J. Mater. Chem. A **11**, 8599 (2023)
11. Q. Lu, K. Eid, W. Li, A.M. Abdullah, G. Xu, R.S. Varma, Green Chem. **23**, 5394 (2021)
12. A. Wang, C. Wang, L. Fu, W. Wong-Ng, Y. Lanecent, Nanomicro Lett. **9**, 47 (2017)
13. V. Shvalagin, S. Kuchmiy, M. Skoryk, M. Bondarenko, O. Khuzhun, Mater. Sci. Eng. B **271**, 115304 (2021)
14. G. Zhang, Y. Xu, C. He, P. Zhang, H. Mi, Appl. Catal. B **283**, 119636 (2021)
15. Y. Zhang, Z. Chen, J. Li, Z. Lu, X. Wang, J. Energy Chem. **54**, 36 (2021)
16. P. Qiu, C. Xu, H. Chen, F. Jiang, X. Wang, R. Lu, X. Zhang, Appl. Catal. B **206**, 319 (2017)
17. F. Wei, Y. Liu, H. Zhao, X. Ren, J. Liu, T. Hasan, L. Chen, Y. Li, B.-L. Su, Nanoscale **10**, 4515 (2018)
18. Y. Shang, Y. Wang, C. Lv, F. Jing, T. Liu, W. Li, S. Liu, G. Chen, Chem. Eng. J. **431**, 133898 (2022)
19. A. Sett, D. Das, D. Banerjee, U.K. Ghorai, N.S. Das, B. Das, K.K. Chattopadhyay, Dalton Trans. **47**, 4501 (2018)
20. F. Yang, V. Kuznietsov, M. Lublow, C. Merschjann, A. Steigert, J. Klaer, A. Thomas, T. Schedel-Niedrig, J. Mater. Chem. A. **1**, 6407 (2013)
21. H. Zhao, H. Yu, X. Quan, S. Chen, Y. Zhang, H. Zhao, H. Wang, Appl. Catal. B **152–153**, 46 (2014)
22. X. Fan, Z. Xing, Z. Shu, L. Zhang, L. Wang, J. Shi, RSC Adv. **5**, 8323 (2015)
23. J. Bi, L. Zhu, J. Wu, Y. Xu, Z. Wang, X. Zhang, Y. Han, Appl. Organomet. Chem. **33**, 5163 (2019)
24. A. Savateev, S. Pronkin, J.D. Epping, M.G. Willinger, C. Wolff, D. Neher, M. Antonietti, D. Dontsova, Chem. Cat. Chem. **9**, 167 (2017)
25. L. Lin, H. Ou, Y. Zhang, X. Wang, ACS Catal. **6**, 3921 (2016)
26. H. Ou, L. Lin, Y. Zheng, P. Yang, Y. Fang, X. Wang, Adv. Mater. **29**, 2 (2017)
27. L. Lin, W. Ren, C. Wang, A.M. Asiri, J. Zhang, X. Wang, Appl. Catal. B **29**, 234 (2018)
28. G. Zhang, L. Lin, G. Li, Y. Zhang, A. Savateev, S. Zafeiratos, X. Wang, M. Antonietti, Angew Chem. Int. **57**, 9372 (2018)
29. N. Andryushina, V. Shvalagin, G. Korzhak, G. Grodzyuk, S. Kuchmiy, M. Skoryk, Appl. Surf. Sci. **475**, 348 (2019)
30. Z. Hong, B. Shen, Y. Chen, B. Lin, B. Gao, J. Mater. Chem. A. **1**, 11754 (2013)
31. S. Kumar, T. Surendar, B. Kumar, A. Baruah, V. Shanker, RSC Adv. **4**, 8132 (2014)
32. H. Zou, X. Yan, J. Ren, X. Wu, Y. Dai, D. Sha, J. Pan, J. Liu, J. Mater. **1**, 340 (2015)
33. V.V. Shvalagin, G.V. Korzhak, S.Y. Kuchmiy, M.A. Skoryk, O.V. Selyshchev, D.R.T. Zahn, J. Photochem. Photobiol. A. **390**, 112295 (2020)
34. T.R. Stara, S.Y. Kuchmii, Theor. Exp. Chem. **58**, 240 (2022)
35. A. Raevskaya, V. Panasiuk, G. Korzhak, O. Stroyuk, S. Kuchmiy, V. Dzhagan, D. Zahn, Catal. Today **284**, 229 (2017)
36. O.L. Stroyuk, O.Y. Rayevska, V.V. Shvalagin, S.Y. Kuchmiy, D.V. Bavykin, E.A. Streltsov, S.K. Poznyak, Photochem. Photobiol. Sci. **12**, 621 (2013)
37. D.V. Bavykin, A.N. Kulak, V.V. Shvalagin, N.S. Andryushina, O.L. Stroyuk, J. Photochem. Photobiol. A **218**, 231 (2011)
38. V. Shvalagin, N. Ermokhina, N. Romanovska, R. Barakov, P. Manorik, V. Sapsay, S. Shcherbakov, O. Poddubnaya, A. Puziy, Res. Chem. Intermed. **45**, 4133 (2019)

Publisher's Note Springer Nature remains neutral with regard to jurisdictional claims in published maps and institutional affiliations.

Authors and Affiliations

Vitaliy Shvalagin[1,2] · Aleksandr Kutsenko[1] · Tetyana Stara[1,3] · Polina Hlukhova[1] · Mykola Skoryk[4] · Stepan Kuchmiy[1]

✉ Vitaliy Shvalagin
vitaliy.shvalagin@gmail.com; vitaliy.shvalagin@mpikg.mpg.de

Aleksandr Kutsenko
askutsenko@ukr.net

Tetyana Stara
tstara@nas.gov.ua; stara_t@ukr.net

Polina Hlukhova
polina012163@gmail.com

Mykola Skoryk
SckorickMA@nas.gov.ua

Stepan Kuchmiy
kuchmiy@inphyschem-nas.kiev.ua

[1] L. Pysarzhevskii Institute of Physical Chemistry of the National Academy of Sciences of Ukraine, 31 Nauky Avenue, Kyiv 03028, Ukraine

[2] Department of Colloid Chemistry, Max Planck Institute of Colloids and Interfaces, Am Muehlenberg 1, 14476 Potsdam, Germany

[3] V. Lashkaryov Institute of Semiconductor Physics of the National Academy of Sciences of Ukraine, 41 Nauky Avenue, Kyiv 03028, Ukraine

[4] NanoMedTech LLC, 68 Antonovicha Str., Kyiv 03150, Ukraine